THE JOURNAL OF PHYSICAL CHEMISTRY B

Feature Article

pubs.acs.org/JPCB

Persistent Ion Pairing in Aqueous Hydrochloric Acid

Marcel D. Baer,[†] John L. Fulton,[†] Mahalingam Balasubramanian,[‡] Gregory K. Schenter,[†] and Christopher J. Mundy*[,†]

[†]Physical Sciences Division, Pacific Northwest National Laboratory, Richland, Washington 99352, United States

[‡]Advanced Photon Source, Argonne National Laboratory, Lemont, Illinois 60439, United States

ABSTRACT: For strong acids, like hydrochloric acid, the complete dissociation into an excess proton and conjugated base as well as the formation of independent solvated charged fragments is assumed. The existence of chloride−hydronium ($Cl^-\cdots H_3O^+$) contact ion pairs even in moderate concentration hydrochloric acid (2.5 m) demonstrates that the counterions do not behave merely as spectators. Through comparison of recent extended X-ray absorption fine structure (EXAFS) measurements to state-of-the-art density functional theory (DFT) simulations, we are able to obtain a unique view into the molecular structure of medium-to-high concentrated electrolytes. Here we report that the $Cl^-\cdots H_3O^+$ contact ion pair structure persists throughout the entire concentration range studied and that these structures differ significantly from moieties studied in microsolvated hydrochloric acid gas phase clusters. Characterizing distinct populations of these ion pairs gives rise to a novel molecular level description of how to view the reaction network for acid dissociation and how it relates to our picture of acid−base equilibria.

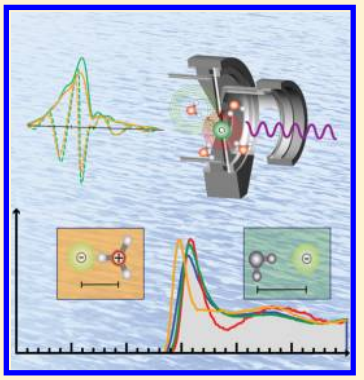

INTRODUCTION

One of the most fundamental concepts in aqueous chemistry is the degree of dissociation or acidity of Brønsted acids. The dissociation, formation of an excess proton and conjugated base, is at the very heart of many condensed phase chemical reactions, ranging from atmospheric, biological, to industrially relevant processes. The dissociation mechanism of a protic acid in water can be viewed as a two step process:

$$\underset{a}{X-H\cdots OH_2} \underset{k_{ba}}{\overset{k_{ab}}{\rightleftharpoons}} \underset{b}{X^-\cdots H-OH_2^+} \underset{k_{cb}}{\overset{k_{bc}}{\rightleftharpoons}} X_{aq}^- + \underset{c}{H_3O_{aq}^+} \quad (1)$$

in which the first step ($a \rightarrow b$) is the proton transfer from the acid (XH) to a hydrogen-bonded water molecule and formation ($b \rightarrow c$) of the resulting fully dissociated anion and cation. The verification of a distinct intermediate species such as the contact ion-pairing between the anion and the formed hydronium (H_3O^+) at moderate concentrations establishes a comprehensive microscopic picture of acids. To this end, we go beyond the usual treatment of a single HCl moiety and proton defect and determine the precise structure and distribution for the complete set of protic species in concentrated electrolytes using ab initio approaches.

There is little doubt that a molecular characterization of the excess proton in aqueous systems is needed to broaden our understanding of fundamental processes in physical chemistry and biology.[1−3] Pioneering studies focusing on a single excess proton, but not the conjugated base, have impacted the way we view the reaction of the aqueous protons based on a molecular picture of the "Eigen" and "Zundel" forms of the excess proton in aqueous systems.[4] Theoretical understanding of this complex is not limited to the classical mechanics but includes the important quantum effects of the shared proton as well.[4]

Here we will depart from the well-characterized single proton defect and determine the structure of aqueous hydrochloric acid over a range of concentrations. Our studies will reveal the significant population of the contact ion pair between the chloride anion and the proton defect ($Cl^-\cdots H_3O^+$) proposed in the original EXAFS study[5] and is shown Figure 1a1. The aforementioned contact ion pair persists even at lower concentrations (e.g., 2.5 m) of aqueous hydrochloric acid mixtures, as proposed in the original study.[5] We also show that our combined molecular dynamics-extended X-ray absorption fine structure (MD-EXAFS) analysis approach[6−10] is consistent with well-established neutron and X-ray diffraction data, yielding a very detailed understanding of the local solvation structure of chloride. Thus, this comparison of different experimental techniques establishes that the well-accepted X-ray and neutron scattering experiments are sensitive to the changes in the solvent structure due to the excess protons. The ability to connect a set of independent experimental measurements to the molecular structures obtained by ab initio molecular dynamics highlights the strength of a "bottom up" approach to statistical mechanics. The analysis put forth in this study provides universal agreement of the structure of concentrated HCl between simulation and three different experimental probes.

We go beyond quantifying the existence of a $Cl^-\cdots H_3O^+$ contact ion pair and assign a unique structure depicted as (b1) in Figure 1, demonstrating that the counterions do not behave merely as spectators but will contribute to an additional stable intermediate molecular state. Although there have been earlier

Received: January 30, 2014
Revised: April 24, 2014

   dx.doi.org/10.1021/jp501091h | J. Phys. Chem. B XXXX, XXX, XXX−XXX

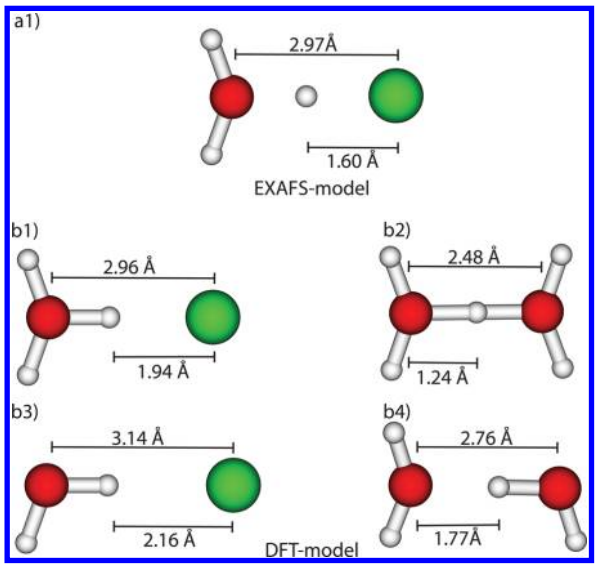

Figure 1. Structural models for the interpretation of the experimental data (a1) is the Zundel-like shared proton. (b1–b4) represent characteristic moieties present in the simulated ensemble. The green circle is a chloride anion and the red and white circles denote oxygen and hydrogen, respectively.

important simulation studies of the concentration-dependent structure in HCl solutions, the experimental determination and subsequent theoretical verification of the preponderance of a stable intermediate state in the acid–base equilibria of HCl was never fully established.[12−16] One specific exception is the study by Heuft and Meijer,[14] and we will relate their findings to those found in this study. In addition, we will demonstrate that the structures found for these more concentrated acid (or electrolyte) solutions cannot be reproduced by the study of water–hydrochloric acid clusters and thus rely on the longer range solvation provided by a disordered liquid phase that will lead to different structural motifs than are inferred from gas phase studies.[17−19] The first high-quality neutron diffraction (ND) and X-ray diffraction (XRD) for a series of concentrated HCl solutions was performed nearly forty years ago by Triolo and Narten (TN).[11] Similar experiments were performed more recently that used a combination of molecular dynamics in conjunction with Lennard-Jones interaction potentials, ND, and XRD to infer a molecular picture of concentrated acids.[20−22] A theoretical analysis of the TN data, performed fifteen years ago by Agmon, concluded that the structures that are consistent with XRD and ND are ringlike, connecting a $H_5O_2^+$ to the chloride anion as shown in Figure 1 of ref 23. Moreover, Agmon also concluded that the higher concentration HCl solutions support a picture where one of the solvating waters of the chloride anion is replaced by HCl forming an "asymmetric bichloride anion", as shown in Figure 2 of ref 23 and found in ab initio simulation studies.[12,13] The additional new information provided by EXAFS points to a key finding that the Cl–$O_{H_3O^+}$ complex will have significantly shorter bond distances between oxygen and chlorine than the Cl–O_{H_2O} (chloride–water oxygen) complexes that are reported in the previous pioneering work by Agmon.[23]

■ RESULTS AND DISCUSSION

When simulating reactive electrolytes such as acids, it is imperative to utilize a force field that reproduces the true

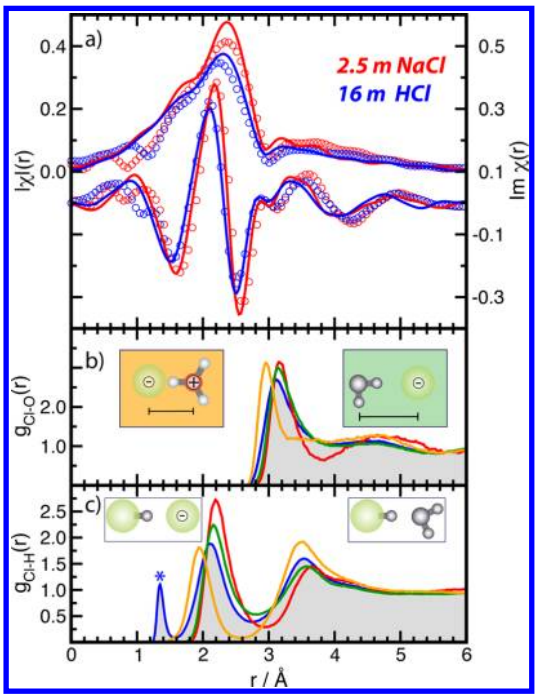

Figure 2. Comparison of EXAFS Cl K-edge (open symbols) and MD-EXAFS (solid lines) spectra for 2.5 m NaCl (red) and 16 m HCl (blue). (a) Top curves correspond to k^2-weighted $|\chi(R)|$ (left axis) and the bottom curves correspond to $\mathrm{Im}[\chi(R)]$ (right axis). The $\mathrm{Im}[\chi(R)]$ is sensitive to the contraction of the Cl–O distance in the formed contact ion pair between hydronium and chloride that is not present in the salt solution. (b and c) depict the simulated pair distribution functions for Cl–O and Cl–H, respectively. The blue-outlined gray-shaded area and the red curve correspond to the HCl and NaCl distributions in accordance with the experiment and simulated EXAFS data in (a). The partial decompositions into Cl–$O_{H_3O^+}$ and Cl–O_{H_2O} are shown in orange and green, respectively, with the structural moieties depicted as insets in (b) (water hydrogens and oxygens are rendered as small and large gray-scaled spheres, respectively. Charge is indicated with "+" or "−", and the choride is rendered as a green sphere). The asterisk appearing above the peak at 1.4 Å in (c) is comprised of structures appearing in the inset of (c).

chemical state in an unbiased fashion. To this end, we employ DFT in conjunction with the sampling protocol described in more detail below. Although there are known shortcomings of DFT when describing weak interactions, there is an emerging consensus that DFT can produce a vastly superior picture of local solvation over the more computationally efficient and commonly used empirical potentials.[9,10,24] Many joint experimental (EXAFS) and theoretical studies have led to a microscopic rationalization of the well-known specific ion effect that is shown to be correlated with the flexibility of the first solvation shell.[25] Going beyond the single-ion picture to deduce the structure of concentrated electrolytes is the next logical step toward assessing the accuracy of DFT methods and thereby probing a regime of multicomponent systems that are at physiologically and industrially relevant concentrations.

Previously, an EXAFS study was performed on a series of HCl concentrations (2.5 to 16 m) to verify the existence of ion pairing between Cl^- and H_3O^+. The main structural assignment of this study is schematically shown in Figure 1a1. This structure is a result of a detailed analysis of the experimental EXAFS data that is shown in Figure 2a. It is the proposed structural model of a Zundel-like shared proton based on the

dx.doi.org/10.1021/jp501091h | J. Phys. Chem. B XXXX, XXX, XXX–XXX

original EXAFS data.[5] Panels (b1−b4) represent characteristic moieties based on the DFT simulation data to assign the X-ray and neutron diffraction data.[11] For clarity, we are only depicting data for the 16 m HCl and the reference 2.5 m NaCl solutions. The full data set can be seen in Figure 3 and in ref 5. The

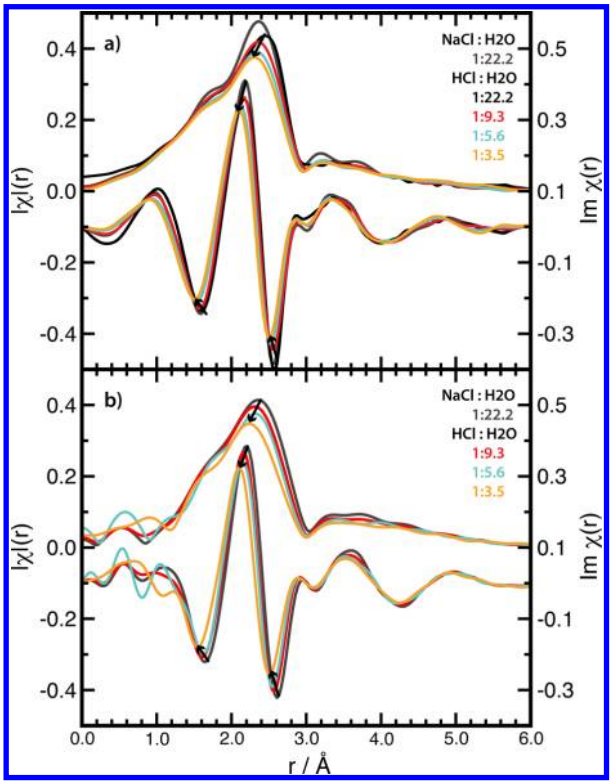

Figure 3. Experimental and theoretical EXAFS Cl K-edge as a function of the concentration of the electrolyte solution. Experimental and theoretical data, respectively (top and bottom). The top curves in each panel correspond to k^2-weighted $|\chi(R)|$ (left axis), and the bottom curves in each panel correspond to $\mathrm{Im}[\chi(R)]$ (right axis). The loss of coordinated oxygens in the first solvation shell are manifest in the change of intensity in the peaks in $|\chi(R)|$ (top curves). The $\mathrm{Im}[\chi(R)]$ (bottom curves) is sensitive to the contraction of the Cl−O distance in the formed contact ion pair between hydronium and chloride that is not present in the salt solution. Ratios of HCl to water of the experiment and simulation are in the legend in each panel. Black arrows are shown as guides to elucidate the evolution of the EXAFS signal to shorter Cl−O distances as a function of increasing acid concentration.

salient feature of the experimental data is the clear shift in the first peak that was assigned to a contracted ion pair $Cl{-}O_{H_3O^+}$ distance of 2.97 Å, as shown in Figure 1 (top panel). The aforementioned moiety is easily distinguished from the $Cl{-}O_{H_2O}$ distance of 3.14 Å in Figure 1b3. With the aid of neutron diffraction data,[11] the Cl−H distance in the EXAFS detected $Cl{-}H{-}O_{H_3O^+}$ ion pair in Figure 1a1 was experimentally assigned to the surprisingly short distance of 1.6 Å, giving the ion pair a Zundel-like quality.[5] Thus, it is the EXAFS predicted structure depicted as (a1) that constitutes the primary basis of our investigation using molecular dynamics (MD) with interaction potentials based on DFT.

Through simulation, we are afforded a close look at underlying populations of different molecular species as a function of concentration. The dominant molecular species are shown in the bottom panel of Figure 1 and will be used in the assignment of spectral signatures. The favorable aspect of EXAFS is that it is only sensitive to changes in local populations of molecular species in the vicinity of the photoelectron source, the chloride anion. To this end, in Figure 2b we decompose the Cl−O radial distribution functions to depict the different atom distances corresponding to the oxygen being either a H_3O^+ or H_2O moiety. Here we use the well-established protocol for analyzing simulations with an excess proton.[4] Performing the decomposition, we find that the $Cl{-}O_{H_3O^+}$ bond distance of 2.96 Å in our simulations (in Figure 1b1) is in good agreement with the experimentally observed value of 2.97 Å (Figure 1a1). Again, all of the relative changes shown in Figure 2 persist throughout the entire concentration range for which we find excellent agreement between our simulations and EXAFS is obtained. Clear differences are seen between the high concentrated acid and the low concentration salt solution. The differences in these spectra are due to the changes in the first solvation shell involving the Cl−O correlations. The loss of coordinated oxygens in the first solvation shell manifest itself in a change of intensity in the peaks in $|\chi(R)|$ (see Table 1 for precise values).

Table 1. Averaged Oxygen Coordination Numbers around Chloride Ions for Hydronium Oxygens ($n_{H_3O^+}$), and Water Oxygens Averaged of All Chloride Ions (n_{H_2O})

	2.5 m NaCl	2.5 m HCl	6 m HCl	10 m HCl	16 m HCl
MD					
n_{H_2O}	5.96	5.82	5.21	4.67	3.99
$n^{3.3Å}_{H_3O^+}$	–	0.13	0.35	0.58	0.82
$n^{3.5Å}_{H_3O^+}$	–	0.17	0.42	0.71	1.05
EXAFS					
n_{H_2O}	6.4	–	5.1 ± 0.5	4.8 ± 0.5	4.2 ± 0.5
$n_{H_3O^+}$	–	–	0.7 ± 0.2	1.0 ± 0.3	1.6 ± 0.3

Figure 2 (panels b and c) denotes the total Cl−O and Cl−H pair distribution functions. The red curve and gray-shaded curve in both panels are the simulated data for the 2.5 m NaCl and 16 m HCl solutions, respectively. We can isolate the contraction of the $Cl^-\cdots H_3O^+$ contact ion pair formed by examining the $Cl{-}O_{H_3O^+}$ distribution (orange curve) and the $Cl{-}O_{H_2O}$ distribution (green curve). The clear shift to shorter distances is readily apparent and is in excellent agreement with the EXAFS data.[5] It is important to point out that contraction of the $Cl^-\cdots H_3O^+$ contact ion pair was first observed in an earlier condensed phase study.[14] However, the radial distribution function for $Cl{-}O_{H_3O^+}$ is dramatically different than the work presented here.[14] Moreover, this earlier study predicts that the solvent-separated ion pair is by far the most prevalent species (at the concentrations of that study − 2.7 and 5.3 m) in contrast to our findings.[14] Earlier multistate empirical valance bond potentials on concentrated HCl clearly show that the $Cl{-}O_{H_3O^+}$ distance is greater than 3 Å.[16,26] Thus, in order to a priori predict a preponderance of the contracted contact ion pair an unbiased representation of the interaction based in quantum mechanics seems to be imperative.

A similar analysis can be performed by examining the total Cl−H populations as shown in Figure 2c. Here one observes an analogous trend. However, as stated earlier, the experimental

dx.doi.org/10.1021/jp501091h | J. Phys. Chem. B XXXX, XXX, XXX−XXX

EXAFS data was assigned the Cl−H distance in the Cl−H−$O_{H_3O^+}$ structure to the significantly shorter distances reminiscent of a Zundel complex (Figure 1a1) that has since been attributed to quantum effects.[19] However, in this DFT study, we do not find a strong delocalization of the shared proton, rather a structure like Figure 1b1 is sufficient to achieve the excellent agreement with the experiment, although changes with concentration in the region near 1 Å in the experimental spectrum in Figure 2a are not reproduced. This important point will be addressed later in the manuscript.

For completeness, we examine the difference in coordinating species around the chloride, namely Figure 1 (b1 versus b3). The aforementioned populations as a function of concentration are tabulated in Table 1. Our findings suggest that the total number of coordinating oxygens is reduced from about 6 at the lowest (2.5 m) to 5 at the highest concentration (16 m), as can be seen by the sum of coordinating water molecules, n_{H_2O}, and hydronium ions, $n_{H_3O^+}$. To determine $n_{H_3O^+}$ in our simulations, we used cutoff of 3.3 Å in accordance with the minimum of the first peak in the radial distribution function of Cl−$O_{H_3O^+}$ at 2.5 m. This is not the same integration range defined by the "Gaussian Approximation" method that is the standard basis for EXAFS modeling.[27] We reconcile these two methods by extending the MD cutoff to 3.5 Å as being a more accurate representation of the EXAFS range. Both integration ranges are presented in Table 1 for completeness. The results in Table 1 lead to a picture that suggests that at the higher concentrations almost all of the chloride are involved in a $Cl^-\cdots H_3O^+$ contact ion pair, with very few free protons distinct from the results at 2.5 m. Table 1 also lists coordination numbers derived from the experimental EXAFS model.[5] The degree of ion pairing here is somewhat higher than in the simulated value, further confirming the important role of this species even at moderate concentrations.

The good agreement between the simulated and the experimental EXAFS data regarding significant populations of the contracted $Cl^-\cdots H_3O^+$ contact ion pair can be further corroborated by revisiting the well-established neutron and X-ray diffraction data of concentrated HCl.[11] It is important to point out why we focus on the TN data instead of more recent experimental XRD and ND.[20−22] As will be shown below, we use a difference method, namely subtracting the radial distribution functions at two different concentrations, to effectively reduce most of the systematic errors in the experimental spectra. The data provided in refs 20−22 unfortunately cannot be evaluated in this format since radial distribution functions generated directly from the experimentally measured structure factor were not reported. Instead, these authors fit the structure factor using a Monte Carlo approach in which empirical potential (i.e., a series of Poisson distributions) is seeded by a starting configuration using the modified Lennard-Jones potential. In this process, the radial distribution functions from the Monte Carlo refinement clearly contain artifacts from the starting empirical potentials. These issues have been noted and discussed in detail in refs 20−22.

The difference spectra are displayed in Figures 4 and 5 (top panels), respectively. Specifically, we subtracted both the experimental and theoretically generated radial distribution functions from the pure water reference at every concentration. Although there are no ambiguities theoretically, some care needs to be exercised when performing the differences for the XRD data. What is shown in Figure 4a is a direct subtraction of the pure water reference. We have also scaled the pure water experimental reference to reflect the proper mole fraction of water at higher acid conentrations. This additional produced negligible differences in the difference spectra. An important aspect of comparing to the earlier X-ray and neutron data is to exploit their very different atom sensitivities for H_2O and Cl and thereby establish the self-consistency of our conclusions regarding the precise structure of concentrated electrolytes. We will demonstrate that the signatures for the contracted Cl−$O_{H_3O^+}$ contact ion pair are present in the X-ray and neutron data that are sensitive to the changes in the structure of water as we increase the electrolyte concentration in Figure 1 (panels b2 and b4). Our results will establish the role of chloride as an active participant in the chemistry that occurs in concentrated HCl solutions.

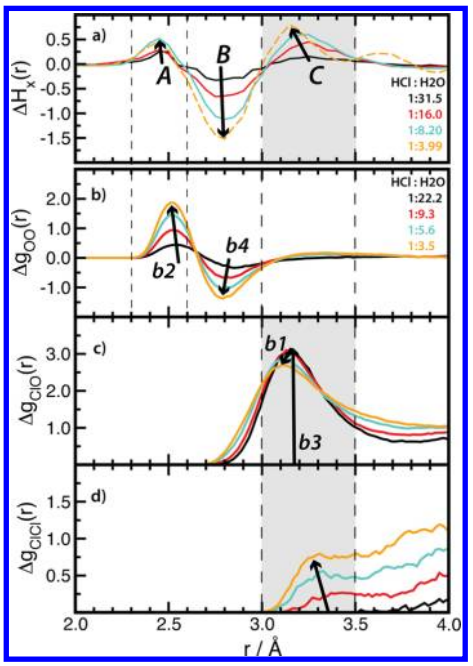

Figure 4. Difference pair-correlation functions at various concentrations of HCl with respect to bulk water: (a) experimental X-ray diffraction data adapted from ref 11; (b−d) simulation data for oxygen−oxygen, chlorine−oxygen, and chlorine−chlorine pairs. The gray highlighted area (feature C in the difference X-ray spectra) correspond to the signature of the contracted Cl−$O_{H_3O^+}$ ion pair that is primarily detected by EXAFS (see Figure 2a). The labels b1−b4 correspond to the structures shown in Figure 1. Ratios of HCl to water of the experiment and simulation are in the upper right-hand corner of (a and b), respectively. The arrows are guides to the eye to show trends with increasing HCl concentration.

In Figure 4a, we present difference X-ray diffraction spectra at different HCl concentrations relative to the pure water spectra.[11] There are three distinct features labeled A, B, and C. Features A and B correspond to the difference in water structure in the presence of the excess proton, namely the loss of water−water pairs depicted by (b4) and the emergence of Eigen/Zundel complexes with a contracted oxygen−oxygen distance represented by (b2). The A and B experimental feature is well-reproduced by the simulated oxygen−oxygen radial distribution function Figure 4b. These structures have been observed in previous independent DFT studies of single proton defects[4] and concentrated HCl solutions.[12,14,15]

dx.doi.org/10.1021/jp501091h | J. Phys. Chem. B XXXX, XXX, XXX−XXX

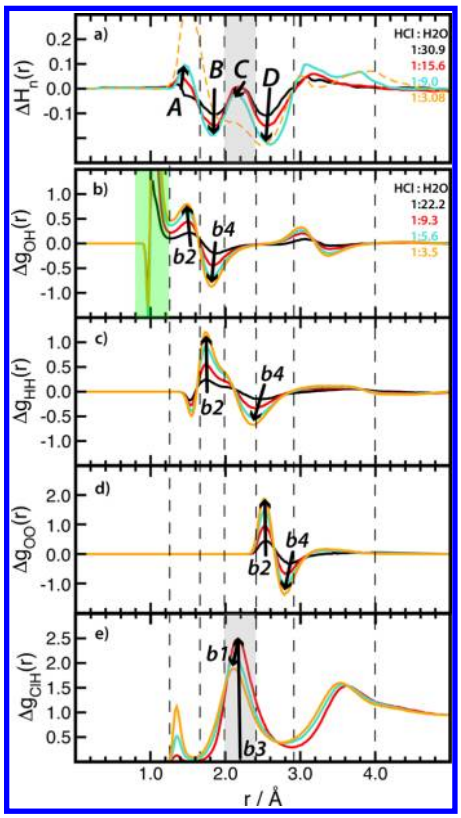

Figure 5. Difference pair-correlation functions at various concentrations of HCl with respect to bulk water (a) experimental neutron diffraction data adapted from ref 11 (b–e) simulation data for oxygen–hydrogen, hydrogen–hydrogen, oxygen–oxygen, and chlorine–oxygen pairs. The highlighted area in gray (feature C in the difference neutron spectra) corresponds to the signature of the contracted Cl–$O_{H_3O^+}$ ion pair that is primarily detected by EXAFS (see Figure 2a). The highlighted area in green in (b) denotes the differences in the internal geometry between proton defect and water. This feature was subtracted out in the original neutron diffraction spectra.[11] The labels b1–b4 correspond to the structures shown in Figure 1. Ratios of HCl to water of the experiment and simulation are in the upper right-hand corner of (a and b), respectively. The arrows are guides to the eye to show trends with increasing HCl concentration.

The EXAFS experimental determination of the contracted Cl–$O_{H_3O^+}$ that is represented in Figure 2a can also be seen in feature C of the difference X-ray diffraction spectra in Figure 4. Feature C in XRD has contributions from both the Cl–O and Cl–Cl distribution functions shown in Figure 4 (panels c and d), respectively. (Again, we have subtracted the pure water values. In the case of Cl–O and Cl–Cl, there is no contribution from pure water). The largest contribution to the feature C is thus the appearance of the contracted Cl–O due to the initial emergence of the (b3) structure followed by its contraction due to the formation of Cl–$O_{H_3O^+}$ of the (b1) structure as we increase the HCl concentration. There are also contributions to feature C seen in the fourth panel of Figure 4, where we observe the appearance of the Cl–Cl pairs. Because the Cl–O and Cl–Cl distances are similar, both will contribute to feature C in the difference X-ray diffraction spectra observed in Figure 4.

Thus, in agreement with earlier work of Agmon,[23] we assign feature A of Figure 4 to the contraction of the O–O for the hydrated proton, ($H_2O{\cdot}H_3O^+$ and $H_5O_3^+$) distance of a $H_5O_3^+$ species b2 in Figure 1. Here we will refrain from denoting this as an Eigen or Zundel complex but will make the distinction that this signal will not involve a chloride anion. It is important to point out that feature C in Figure 4 shows a shortening that is consistent with the contracted contact ion pair (b1) in Figure 1 and is in near quantitative agreement with the total Cl–O radial distribution function in Figure 4c that contains the correct populations of moiety b1. The other interesting structured feature from simulated concentrated HCl studies is the possible existence of an "asymmetric bichloride" ion that is shown in Figure 2 (left inset in panel c).[12,13] The purported Cl–Cl peak in the XRD [11] that should lead to a strong EXAFS signal was not observed in Figure 2. The lack of such a feature in the EXAFS data in Figure 2 is consistent with a very disordered Cl–Cl interaction, as shown in the radial distribution function in Figure 4d. Certainly there exists moieties that resemble combinations of associated HCl–water (see Figure 2, right inset of panel c) and the aforementioned bichloride anion in Cl–H radial distribution function in Figure 2. However, our simulations suggest that these disordered species are transition states between the stable structures that are reported in Figure 1.

Signatures of the contracted $Cl^-\cdots H_3O^+$ contact ion pair observed in the EXAFS data are also present in the neutron diffraction data shown in Figure 5. Again, Figure 5 shows both the difference neutron spectra and pair distribution functions as a function of HCl concentration relative to the pure water reference data. The difference neutron spectra show four features labeled A–D. We first focus our attention on the green highlighted region below 1.2 Å in the difference of the total H–O distribution functions from our simulations. This contribution from the intramolecular O–H scattering was removed in the experimental treatment and therefore no direct comparison is possible for water molecule short bonds on the order of 1 Å.[11] Features A and B in the difference neutron spectra shown in Figure 5 are again largely correlated to the perturbed water structure due to the excess proton as discussed above. Feature C in the difference neutron spectra can be correlated to the corresponding region in the difference of the total Cl–H distributions in Figure 5e. Here, there is a clear contraction to shorter distances due to the building in of structures resembling (b1) and a reduction (b4) as the concentration of HCl is increased in agreement with the interpretation of the EXAFS data shown in Figure 2a.

Last, feature D in the difference neutron spectra can be attributed to the change in water structure as one increases the concentration of excess protons shown in Figure 5 (panels c and d). As in the difference X-ray data in Figure 4, there is a loss of (b4) moieties accompanied by an increase in (b2) structures. However, in the difference neutron spectra, the direct correlation to individual difference pair correlation function is confounded due to the overlapping contributions from O–O, O–H, and H–H distributions. Note the color code for the experimental and simulated concentrations are different.

We now turn the discussion toward the role of nuclear quantum effects in the detailed structure of the contracted $Cl^-\cdots H_3O^+$ contact ion pair. In a recent paper, a cluster study using four water molecules was carefully chosen to stabilize the contracted $Cl^-\cdots H_3O^+$ contact ion pair.[19] In this study, it was reported that significant difference in the total Cl–$H_{H_3O^+}$ distance was seen when path integral treatment of the proton

dx.doi.org/10.1021/jp501091h | J. Phys. Chem. B XXXX, XXX, XXX–XXX

was utilized in good agreement with the fitted EXAFS model.[5,19] For this reason, a comparison was made of the influence of nuclear quantum effects in a four water cluster system versus bulk system using classical phase-space analysis. In the future, this understanding will be put to a firmer foundation using direct path integral simulation methods. The phase-space analysis highlights the essential differences between the cluster and bulk systems regarding the role of anharmonicity. It also serves as a self-consistent check on the results obtained using a full path integral analysis of clusters.[19] Density functional theory calculations were performed using the identical code and protocol as in ref 19. To this end, the phase-space analysis was performed by examining the position and velocity projected along the Cl−H−O moiety comprising the contact ion pair. The results of the cluster study juxtaposed on the condensed phase study at 2.5 m is shown in Figure 6.

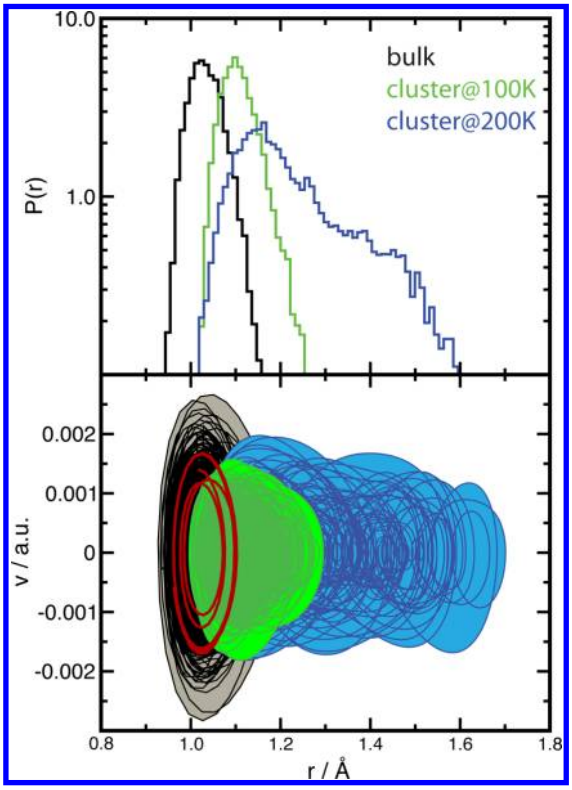

Figure 6. Phase-space analysis projected along the Cl−H−O distance as a function of simulation protocol, namely the condensed phase versus the four water cluster performed in ref 19. The left panel depicts the populations of the H−O distance.

The top panel of Figure 6 is the distribution of O−H distances along the projected coordinate. One can see distinct differences in the population between the condensed phase calculations at 300 K and the 100 K cluster calculations, namely the O−H distance in the cluster calculation is shifted to significantly longer distances. This, in-and-of-itself may not be surprising but with the hindsight afforded by the full path integral calculation,[19] could be regarded as a signature that the bulk and cluster studies yield significantly different structures. To explore this conjecture, we performed a calculation at 200 K in the cluster. In the 200 K trajectory, it is seen that dramatic anharmonic effects are present. These can be characterized by a phase-space analysis. The 200 K O−H populations are significantly distorted and the phase-space analysis depicts orbits in a "figure 8" pattern that suggest large amplitude motions are accessible through quantum effects such as zero-point delocalization at 100 K. Given the well-converged results in ref 19, it is reassuring that the signatures of quantum mechanical behavior can be captured by a simpler analysis and distinct differences between cluster and condensed phase calculations of ion-pairing in aqueous HCl can be observed. In contrast, the bulk simulations reveal a much more confined effective potential even at 300 K. Specifically, we do not see large anharmonic motions in the phase-space analysis in the condensed phase. We considered the effective potential along the O−H coordinate as a one-dimensional system and solved the corresponding Schrödinger equation. In doing so, we find that the shift in the mean position relative to the minimum position to be insignificant compared to the anharmonic shifts seen in the classical cluster motion. The good agreement between the MD-EXAFS and EXAFS data obtained in the condensed phase calculation under classical mechanics is further indication that the quantum effects may not play a significant role in the structure of the Cl−H−O contact ion pair. It should be pointed out that the phase-space analysis presented here is only an indirect confirmation regarding the role of quantum effects in the Cl−H−O contact ion pair in the condensed phase. We do not rule out the role that quantum effects may have regarding the precise populations of Eigen- versus Zundel-like contracted ion pairs pending a full quantum treatment in the condensed phase.

Finally we explore the source of dissimilarities between the simulated and the experimental EXAFS structures. The earlier EXAFS paper detects the backscattering of the Cl−H proton at 1.6 Å that was assigned to a structural feature of a Zundel-like contact ion pair. This signal appears in the region of the $\chi(r)$ plot in Figure 2a at about 1 Å (distance not corrected in the plot for the photoelectron phase shift). This EXAFS feature is supported by the neutron diffraction result showing a peak at 1.5 Å in Figure 5. We conjecture that there is an interesting possible reassignment for the Cl−H distance at 1.5−1.6 Å, seen in the EXAFS data. This feature could be rather related to the Cl−H peak at 1.4 Å in the distribution function in Figure 2c. The possible structural moieties that make up the aforementioned peak are shown as insets in Figure 2c. The EXAFS error in distances could be due to the FEFF estimate of the Cl−H muffin tin overlap radii that is usually only optimized for O−H bonds of water.[9]

Overall, we have combined two distinct experimental views of electrolytes, namely the perturbation of the water structure due to the excess protons probed with neutron and X-ray diffraction, with the perturbation of the local structure due to the counterion as determined by EXAFS. We have established that combining these views is necessary to properly understand the structure of concentrated electrolytes.

■ CONCLUSIONS

In summary, we find excellent agreement between our state-of-the-art DFT calculations coupling to statistical sampling and the recent EXAFS data and existing neutron and X-ray diffraction data of concentrated HCl solutions. Indeed, when we include the new structural information of the electrolyte from the point-of-view of the counterion (as the EXAFS photo electron source), a rich picture emerges regarding the role of the chloride anion as an active participant in the chemistry of concentrated HCl solutions. We are in agreement with the

dx.doi.org/10.1021/jp501091h | J. Phys. Chem. B XXXX, XXX, XXX−XXX

original interpretation of the EXAFS proposed molecular structure based on the Cl−$O_{H_3O^+}$ distance.

The importance of an intermediate species *b* in eq 1 has implications for many processes that take place at interfaces. It was noted in a previous study that acids, such as HNO_3, at interfaces behave like their high-concentration counterparts in bulk.[28,29] Moreover, it is known that acids (i.e., HNO_3) can exist in their molecular forms in the vicinity of the air−water interface.[28−31] For HCl, there is some evidence that there is a short-lived molecular complex on surfaces such as glycerol.[32−34] However, there is no spectroscopic evidence that HCl exists in the pure molecular at the surface of water.[35] Nevertheless, the possibility for characterization of molecular acids or distinct contact ion pairs as put forth in this study at the air−water interface will impact the way we view the surfaces of acid electrolytes. The preponderance of these correlated contracted contact ion pairs found for HCl in this study points to the possibility that similar species could be present in the vicinity of the interface.[36] This study suggests that the intrinsic potentials of mean force of the excess proton may not be enough to understand whether the air−water interface is more acidic or basic.[37−40] Moreover, empirical models should be flexible enough to contain the possibilities of these distinct equilibrium states in eq 1.[16,36,41,42] Thus, future studies of acids at the air−water interface using the protocol outlined herein are an obvious next step.

Regarding the role of quantum effects, we do not find a Zundel-like shared proton depicted in (a1) to fit the experimental EXAFS data.[5,19] Rather, the picture from this study supports the Eigen-like contracted ion pair (b1) in Figure 1 that is unique to the bulk solvation of the chloride anion. It must be emphasized that although our phase-space analysis supports the large shifts in the Cl−$H_{H_3O^+}$ found in the path integral calculations of ref 19, it is an indirect confirmation and we cannot completely rule out large amplitude anharmonic motions in the Cl−$H_{H_3O^+}$ distance in the 300 K condensed phase calculations presented herein. Although quantum effects seem to play a significant role in crystals of HCl hydrates[43] and microsolvated HCl,[19] understanding these quantum effects in the presence of a strong asymmetric environment with large fluctuations that are not present in the aforementioned studies is future research.

Nevertheless, we leave ourselves completely open to the role of quantum effects regarding the precise populations of Eigen- versus Zundel-like contracted contact ion pairs pending a proper full quantum treatment of concentrated HCl in the condensed phase. Future experimental studies regarding the lifetimes of the contracted Cl−$O_{H_3O^+}$ ion pair and their dynamical correlations will be important to complete the picture put forth in this study. Our MD-EXAFS analysis in conjunction with pair correlation functions suggests a picture of persistent ion pairing in concentrated acid solutions even at moderate concentrations. Thus, establishing the role of the chloride counterion as an active participant in the chemistry that determines the pH scale.

MATERIALS AND METHODS

We directly compare the experimental EXAFS structure to the MD structure using the method of molecular dynamics EXAFS (MD-EXAFS).[6−8] In EXAFS analysis, it is common to fit experimental measurement to a single effective structure that represents the average of the locally fluctuating structure. In contrast, the full MD-EXAFS procedure takes into account the full, multidimensional molecular detail by calculating an EXAFS spectrum from atomic coordinates of all frames of the simulation using an ab initio scattering code (FEFF9).[44,45] This ensemble average spectrum then provides an exact representation of the local structure, since it contains contribution from all of the EXAFS photoelectron single- and multiple-scattering process about the central absorbing Cl atom.

We compare five different systems, 2.5 m NaCl and 2.5, 6, 10, and 16 m HCl. Experimental details are described in ref 9. The CP2K simulation suite (http:www.cp2k.sourceforge.net) containing the QuickStep module for the DFT calculations is utilized.[46] Our basic simulation setup consists of supercells that are chosen to reproduce the experimental density of 2.5, 6, 10, and 16 m HCl and 2.5 m NaCl. All simulations are charge neutral. The linear supercell dimension for 2.5 m NaCl is 15.218 Å, which comprised of 111 water molecules and 5 NaCl pairs. The linear supercell dimension for the HCl solutions are 15.175, 15.702, 15.786, and 15.842 Å for the 2.5, 6, 10, and 16 m solutions, respectively. Furthermore, the HCl simulations contained 111 waters and 5 HCl, 115 waters and 12 HCl, 107 waters and 20 HCl, 99 waters and 28 HCl for the 2.5, 6, 10, and 16 m solutions, respectively. All calculations used a plane-wave cutoff for the density of 280 Rydbergs. We used the exchange functional due to Becke[47] and correlation due to Lee, Yang, and Parr (BLYP).[48] We augmented the BLYP functional with the dispersion correction due to Grimme.[49] This combination, referred to as BLYP-D, has been shown to produce more satisfactory structural, dynamical, and thermodynamic properties of liquid water near ambient conditions.[50,51] For our Gaussian basis set we used a double-ζ quality optimized for the condensed phase.[52] The aforementioned protocol has been shown by us to provide excellent agreement with EXAFS data regarding the local structure of both simple and polyatomic anions.[9,10,25] Moreover, we have examined improvements of gradient-corrected functionals, namely hybrid functionals such as PBE0 to study the hydration structure of cations benchmarked against EXAFS data.[24] For six cations, the average improvement amounted to 0.020 Å in the oxygen−cation distance. In a more recent study, a one-to-one comparison between PBE0 and PBE was performed for the hydration structure of chloride.[53] The apparent improvement is about 0.040 Å for PBE0. With our choice of BLYP-D, the predicted Cl−O_{H_2O} and Cl−$O_{H_3O^+}$ distances of 3.14 and 2.97 Å, respectively, are within 0.010 Å of the value measured by EXAFS. Thus, there is excellent agreement between the predicted and measured structure that should be robust with further improvements of the BLYP functional.

To equilibrate the system under the assumption that hydrochloric acid is a strong acid, an adiabatic sampling technique[54,55] is used to enhance, while the chlorine diffusion and the number of protons closer than 1.3 Å are restrained to be zero using coordination restraints. Our separation of timescales is predicated on the assumption that chloride diffusion is "slow" with respect to the solvent reorganization (including the proton defect). To this end, we use a chlorine mass of 500 amu and an elevated temperature of 2000 K. The water and proton defect are simulated with the default masses and at a temperature of 300 K. To maintain the desired adiabatic separation, a Nosé-Hoover Chains thermostat was

dx.doi.org/10.1021/jp501091h | J. Phys. Chem. B XXXX, XXX, XXX−XXX

used on every degree of freedom at a frequency of 2300 cm^{-1} for both subsystems.[56] Thus, for equilibration purposes we view the chloride−chloride interaction as if it were mediated through a dielectric containing water and the proton defect. Indeed, reweighted chloride−chloride distribution functions would give rise to their equilibrium structure and potentials of mean force. However, for our purposes herein, we use the aforementioned sampling method to produce an ensemble of initial conditions to then run standard unbiased ab initio molecular dynamics. These assumptions, will of course, be justified by direct comparison to experiment. Each system is equilibrated under the adiabatic sampling setup for 20 ps. Four individual initial configurations taken 4 ps apart were harvested from the equilibration period and run unrestrained, standard molecular dynamics in the NVT-ensemble for 20 ps.

To make direct contact with the EXAFS experiment, simulations of aqueous hydrochloric acid are performed at the experimental densities and concentrations corresponding to 2.5, 6, 10, and 16 m solutions of HCl. In order to provide a proper benchmark for the distance contraction of $Cl-O_{H_3O^+}$ heavy atoms, we performed formed simulations at the experimental conditions of 2.5 m solution of NaCl. The comparison of the EXAFS spectra obtained from DFT and the experimentally observed spectra for 2.5 m NaCl is shown in red in Figure 2a. One can see excellent agreement with the features of the experiment. Moreover, the quality of agreement for the DFT simulation of a concentrated electrolyte gives credibility to the methods and simulation protocols described above. The salient result is that we can reproduce the $Cl-O_{H_2O}$ distance of 3.14 Å as deduced by experiment. We can now proceed to the concentration series of the reactive hydrochloric acid. Here, as shown in Figure 2a once again, we can see excellent agreement with the experimental EXAFS at the highest concentration of 16 m. This also gives us confidence in our simulation protocol to faithfully reproduce the correct populations of $Cl-O_{H_3O^+}$ contact ions pairs and fully dissociated HCl giving rise to near quantitative agreement with first solvation shell structure as measured by the experiment.

AUTHOR INFORMATION

Corresponding Author

*E-mail: chris.mundy@pnnl.gov.

Notes

The authors declare no competing financial interest.

Biographies

Marcel Baer has been a Staff Scientist at Pacific Northwest National Laboratory (PNNL) since 2014. Prior to this, Baer was a Linus Pauling Distinguished Postdoctoral Fellow at PNNL from 2011 to 2014. Baer's interests are in the fundamentals of spectroscopy and understanding the origins of the specific ion effect. Baer received is Ph.D. in Theoretical Chemistry in 2010 from Ruhr-Universität in Bochum, Germany, under the direction of Prof. Dominik Marx.

John Fulton is currently a Staff Scientist in the Physical Sciences Division of Pacific Northwest National Laboratory. He has published over 120 papers dealing with the structure of ions and multimolecular aggregates in condensed phases under both ambient and extreme conditions. His research interests are focused on developing a molecular-level understanding of the structure and dynamics of both ion/water and ion/ion interactions. He employs methods such as X-ray absorption fine structure (XAFS) spectroscopy, high-energy X-ray scattering (HEXS), coupled with theoretical methods such as DFT-molecular dynamics (MD-XAFS) in order to test and refine structural models of these systems. He holds a M.S. in Chemical Engineering from the University of Washington in 1985.

Dr. Mahalingam Balasubramanian is a physicist in the X-ray Science Division at Argonne National Laboratory. His recent research, using synchrotron techniques, has addressed fundamental questions in energy sciences with emphasis on Li-ion and beyond Li-ion energy storage systems, hydrogen storage materials, solvation structure of ions in aqueous and nonaqueous solvents, electrocatalysts, and the like. He is also involved in the general operation, maintenance, and user support in the XSD-PNC beamlines at Argonne's Advanced Photon Source. He received a Ph.D. (Physics) in 1996 from the University of Connecticut, Storrs.

Dr. Gregory Schenter has been with Pacific Northwest National Laboratory (PNNL) since 1988 and was named a Laboratory Fellow in 2009. Dr. Schenter's research focuses on the development of statistical mechanical techniques to better understand molecular interactions and molecular processes in complex condensed-phase systems. Schenter received his Ph.D. in Applied Physics from Cornell University in 1988.

Christopher J. Mundy has been a Chief Scientist at Pacific Northwest National Laboratory since 2006. Mundy's interests are in combining statisitcal mechanics with quantum density functional theory to obtain a molecular understanding of solvation and the specific ion effect. Mundy received his Ph.D. in Physical Chemistry in 1992 from the University of California, Berkeley.

■ ACKNOWLEDGMENTS

This work was supported the U.S. Department of Energy's (DOE) Office of Basic Energy Sciences, Division of Chemical Sciences, Geosciences and Biosciences. Pacific Northwest National Laboratory (PNNL) is operated for the Department of Energy by Battelle. M.D.B. is grateful for the support of the Linus Pauling Distinguished Postdoctoral Fellowship Program at PNNL. PNC/XSD facilities at the Advanced Photon Source and research at these facilities are supported by the U.S. Department of Energy Basic Energy Sciences, a Major Resources Support grant from NSERC, the University of Washington, the Canadian Light Source, and the Advanced Photon Source. Use of the Advanced Photon Source, an Office of Science User Facility operated for the U.S. Department of Energy (DOE) Office of Science by Argonne National Laboratory, was supported by the U.S. DOE under Contract DE-AC02-06CH11357. This research used resources of the National Energy Research Scientific Computing Center, which is supported by the Office of Science of the U.S. Department of Energy under Contract DE-AC02-05CH11231. We acknowlege computer resources through PNNL's institutional computing (PIC). We acknowledge Gil Nathanson's critical analysis of this work.

■ REFERENCES

(1) Gust, D.; Moore, T.; Moore, A. Mimicking photosynthetic solar energy transduction. *Acc. Chem. Res.* **2001**, *34*, 40−48.
(2) Cukierman, S. Et tu, Grotthuss! and other unfinished stories. *Biochim. Biophys. Acta, Bioenerg.* **2006**, *1757*, 876−885.
(3) Voth, G. Computer simulation of proton solvation and transport in aqueous and biomolecular systems. *Acc. Chem. Res.* **2006**, *39*, 143−150.
(4) Marx, D.; Chandra, A.; Tuckerman, M. E. Aqueous basic solutions: Hydroxide solvation, structural diffusion, and comparison to the hydrated proton. *Chem. Rev.* **2010**, *110*, 2174−2216.
(5) Fulton, J. L.; Balasubramanian, M. Structure of hydronium (H3O +)/Chloride (Cl−) contact ion pairs in aqueous hydrochloric acid solution: A Zundel-like local configuration. *J. Am. Chem. Soc.* **2010**, *132*, 12597−12604.
(6) Palmer, B. J.; Pfund, D. M.; Fulton, J. L. Direct modeling of EXAFS spectra from molecular dynamics simulations. *J. Phys. Chem.* **1996**, *100*, 13393−13398.
(7) McCarthy, M. I.; Schenter, G. K.; Chacon Taylor, M. R.; Rehr, J. J.; Brown, G. E. Prediction of extended x-ray-absorption fine-structure spectra from molecular interaction models: Na+(H2O)(n)-MgO (100) interface. *Phys. Rev. B* **1997**, *56*, 9925−9936.
(8) Dang, L. X.; Schenter, G. K.; Glezakou, V.-A.; Fulton, J. L. Molecular simulation analysis and X-ray absorption measurement of Ca2+, K+ and Cl− ions in solution. *J. Phys. Chem. B* **2006**, *110*, 23644−23654.
(9) Fulton, J. L.; Schenter, G. K.; Baer, M. D.; Mundy, C. J.; Dang, L. X.; Balasubramanian, M. Probing the hydration structure of polarizable halides: A multiedge XAFS and molecular dynamics study of the iodide anion. *J. Phys. Chem. B* **2010**, *114*, 12926−12937.
(10) Baer, M. D.; Pham, V.-T.; Fulton, J. L.; Schenter, G. K.; Balasubramanian, M.; Mundy, C. J. Is iodate a strongly hydrated cation? *J. Phys. Chem. Lett.* **2011**, *2*, 2650−2654.
(11) Triolo, R.; Narten, A. H. Diffraction pattern and structure of aqueous hydrochloric-acid solutions at 20 degreesc. *J. Chem. Phys.* **1975**, *63*, 3624−3631.
(12) Laasonen, K. E.; Klein, M. L. Ab initio study of aqueous hydrochloric acid. *J. Phys. Chem. A* **1997**, *101*, 98−102.
(13) Sillanpaa, A.; Laasonen, K. Structure and dynamics of concentrated hydrochloric acid solutions. A first principles molecular dynamics study. *Phys. Chem. Chem. Phys.* **2004**, *6*, 555−565.
(14) Heuft, J. M.; Meijer, E. J. A density functional theory based study of the microscopic structure and dynamics of aqueous HCl solutions. *Phys. Chem. Chem. Phys.* **2006**, *8*, 3116−3123.
(15) Murakhtina, T.; Heuft, J.; Meijer, E. J.; Sebastiani, D. First principles and experimental H-1 NMR signatures of solvated ions: The case of HCl(aq). *ChemPhysChem* **2006**, *7*, 2578−2584.
(16) Xu, J. Q.; Izvekov, S.; Voth, G. A. Structure and dynamics of concentrated hydrochloric acid solutions. *J. Phys. Chem. B* **2010**, *114*, 9555−9562.
(17) Gutberlet, A.; Schwaab, G.; Birer, O.; Masia, M.; Kaczmarek, A.; Forbert, H.; Havenith, M.; Marx, D. Aggregation-induced dissociation of HCl(H2O)(4) below 1 K: The smallest droplet of acid. *Science* **2009**, *324*, 1545−1548.
(18) Zwier, T. S. Squeezing the Water Out of HCl(aq). *Science* **2009**, *324*, 1522−1523.
(19) Walewski, L.; Forbert, H.; Marx, D. Quantum induced bond centering in microsolvated HCl: Solvent separated versus contact ion pairs. *J. Phys. Chem. Lett.* **2011**, *2*, 3069−3074.
(20) Botti, A.; Bruni, F.; Imberti, S.; Ricci, M. A.; Soper, A. K. Ions in water: The microscopic structure of a concentrated HCl solution. *J. Chem. Phys.* **2004**, *121*, 7840−7848.

(21) Botti, A.; Bruni, F.; Ricci, M. A.; Soper, A. K. Eigen versus Zundel complexes in HCl-water mixtures. *J. Chem. Phys.* **2006**, *125*, 014508.
(22) Mancinelli, R.; Sodo, A.; Bruni, F.; Ricci, M. A.; Soper, A. K. Influence of concentration and anion size on hydration of H+ ions and water structure. *J. Phys. Chem. B* **2009**, *113*, 4075−4081.
(23) Agmon, N. Structure of concentrated HCl solutions. *J. Phys. Chem. A* **1998**, *102*, 192−199.
(24) Fulton, J. L.; Bylaska, E. J.; Bogatko, S.; Balasubramanian, M.; Cauet, E.; Schenter, G. K.; Weare, J. H. Near-quantitative agreement of model-free DFT-MD predictions with XAFS observations of the hydration structure of highly charged transition-metal ions. *J. Phys. Chem. Lett.* **2012**, *3*, 2588−2593.
(25) Baer, M. D.; Mundy, C. J. An ab initio approach to understanding the specific ion effect. *Faraday Disscuss.* **2013**, *160*, 89−101.
(26) Chen, H.; Xu, J.; Voth, G. A. Unusual hydrophobic interactions in acidic aqueous solutions. *J. Phys. Chem. B* **2009**, *113*, 7291−7297.
(27) Glezakou, V. A.; Chen, Y. S.; Fulton, J. L.; Schenter, G. K.; Dang, L. X. Electronic structure, statistical mechanical simulations, and EXAFS spectroscopy of aqueous potassium. *Theor. Chem. Acc.* **2006**, *115*, 86−99.
(28) Lewis, T.; Winter, B.; Stern, A. C.; Baer, M. D.; Mundy, C. J.; Tobias, D. J.; Hemminger, J. C. Dissociation of strong acid revisited: X-ray photoelectron spectroscopy and molecular dynamics simulations of HNO3 in water. *J. Phys. Chem. B* **2011**, *115*, 9445−9451.
(29) Lewis, T.; Winter, B.; Stern, A. C.; Baer, M. D.; Mundy, C. J.; Tobias, D. J.; Hemminger, J. C. Does nitric acid dissociate at the aqueous solution surface? *J. Phys. Chem. C* **2011**, *115*, 21183−21190.
(30) Shamay, E. S.; Buch, V.; Parrinello, M.; Richmond, G. L. At the water's edge: Nitric acid as a weak acid. *J. Am. Chem. Soc.* **2007**, *129*, 12910.
(31) Blower, P. G.; Shamay, E.; Kringle, L.; Ota, S. T.; Richmond, G. L. Surface behavior of malonic acid adsorption at the air/water interface. *J. Phys. Chem. A* **2013**, *117*, 2529−2542.
(32) Chorny, I.; Benjamin, I.; Nathanson, G. Scattering, trapping, and ionization of HCl at the surface of liquid glycerol. *J. Phys. Chem. B* **2004**, *108*, 995−1002.
(33) Krebs, T.; Nathanson, G. M. Reactions of HCl and D2O with Molten Alkali Carbonates. *J. Phys. Chem. A* **2011**, *115*, 6317.
(34) Brastad, S. M.; Nathanson, G. M. Molecular beam studies of HCl dissolution and dissociation in cold salty water. *Phys. Chem. Chem. Phys.* **2011**, *13*, 8284−8295.
(35) Baldelli, S.; Schnitzer, C.; Shultz, M. First spectroscopic evidence for molecular HCl on a liquid surface with sum frequency generation. *J. Chem. Phys.* **1998**, *108*, 9817−9820.
(36) Wick, C. D. HCl accommodation, dissociation, and propensity for the surface of water. *J. Phys. Chem. A* **2013**, *117*, 12459−12467.
(37) Dang, L. Solvation of the hydronium ion at the water liquid/vapor interface. *J. Chem. Phys.* **2003**, *119*, 6351−6353.
(38) Wick, C. D.; Dang, L. X. Investigating hydroxide anion interfacial activity by classical and multistate empirical valence bond molecular dynamics simulations. *J. Phys. Chem. A* **2009**, *113*, 6356−6364.
(39) Jagoda-Cwiklik, B.; Cwiklik, L.; Jungwirth, P. Behavior of the eigen form of hydronium at the air/water interface. *J. Phys. Chem. A* **2011**, *115*, 5881−5886.
(40) Wick, C. D. Hydronium behavior at the air-water interface with a polarizable multistate empirical valence bond model. *J. Phys. Chem. C* **2012**, *116*, 4026−4038.
(41) Petersen, M.; Iyengar, S.; Day, T.; Voth, G. The hydrated proton at the water liquid/vapor interface. *J. Phys. Chem. B* **2004**, *108*, 14804−14806.
(42) Iuchi, S.; Chen, H.; Paesani, F.; Voth, G. A. Hydrated excess proton at water-hydrophobic interfaces. *J. Phys. Chem. B* **2009**, *113*, 4017−4030.
(43) Hassanali, A. A.; Cuny, J.; Ceriotti, M.; Pickard, C. J.; Parrinello, M. The fuzzy quantum proton in the hydrogen chloride hydrates. *J. Am. Chem. Soc.* **2012**, *134*, 8557−8569.
(44) Zabinsky, S. I.; Rehr, J. J.; Ankudinov, A.; Albers, R. C.; Eller, M. J. Multiple-scattering calculations of X-ray-absorption spectra. *Phys. Rev. B* **1995**, *52*, 2995−3009.
(45) Rehr, J. J.; Albers, R. C. Theoretical approaches to X-ray absorption fine structure. *Rev. Mod. Phys.* **2000**, *72*, 621−654.
(46) VandeVondele, J.; Krack, M.; Mohamed, F.; Parrinello, M.; Chassaing, T.; Hutter, J. QUICKSTEP: Fast and Accurate Density Functional Calculations using a Mixed Gaussian and Plane Waves Approach. *Comput. Phys. Commun.* **2005**, *167*, 103−128.
(47) Becke, A. D. Density-Functional Exchange-Energy Approximation with Dorrect Asymptotic Behavior. *Phys. Rev. A* **1988**, *38*, 3098−3100.
(48) Lee, C.; Yang, W.; Parr, R. G. Development of the Colle-Salvetti correlation-energy formula into a functional of the electron density. *Phys. Rev. B* **1988**, *37*, 785−789.
(49) Grimme, S. Accurate description of Van der Waals complexes by density functional theory including empirical corrections. *J. Comput. Chem.* **2004**, *25*, 1463−1473.
(50) Schmidt, J.; VandeVondele, J.; Kuo, I.-F. W.; Sebastiani, D.; Siepmann, J. I.; Hutter, J.; Mundy, C. J. Isobaric-isothermal molecular dynamics simulations utilizing density functional theory: An Assessment of the structure and density of water at near-ambient conditions. *J. Phys. Chem. B* **2009**, *113*, 11959−11964.
(51) Baer, M. D.; Mundy, C. J.; McGrath, M. J.; Kuo, I. F. W.; Siepmann, J. I.; Tobias, D. J. Re-examining the properties of the aqueous vapor-liquid interface using dispersion corrected density functional theory. *J. Chem. Phys.* **2011**, *135*, 124712.
(52) VandeVondele, J.; Hutter, J. Gaussian basis sets for accurate calculations on molecular systems in gas and condensed phases. *J. Chem. Phys.* **2007**, *127*, 114105.
(53) Zhang, C.; Pham, T. A.; Gygi, F.; Galli, G. Communication: Electronic structure of the solvated chloride anion from first principles molecular dynamics. *J. Chem. Phys.* **2013**, *138*, 181102.
(54) VandeVondele, J.; Röthlisberger, U. Canonical adiabatic free energy sampling (CAFES): A novel method for the exploration of free energy surfaces. *J. Phys. Chem. B* **2002**, *106*, 203−208.
(55) Cuendet, M. A.; Tuckerman, M. E. Alchemical free energy differences in flexible molecules from thermodynamic integration or free energy perturbation combined with driven adiabatic dynamics. *J. Chem. Theory Comput.* **2012**, *8*, 3504−3512.
(56) Martyna, G. J.; Klein, M. L.; Tuckerman, M. E. Nose-Hoover chains: The canonical ensemble via continous dynamics. *J. Chem. Phys.* **1992**, *97*, 2635−2643.